Fabrication and Characterization of a Thick-GEM Detector

A Project Report Submitted
in Partial Fulfilment of the Requirements
for the Degree of

MASTER OF SCIENCE

by

Danush S

to the

School of Physical Sciences

National Institute of Science Education and Research

Bhubaneswar

November 26, 2021

ACKNOWLEDGEMENTS

My first thanks go to Prof. Bedangadas Mohanty for providing me the opportunity to work under his guidance for this project. I could not have asked for a better guide and mentor for this project.

I thank Dr. Varchaswi K S Kashyap for his guidance and for bearing a lot of my amateur and sometimes stupid doubts I have asked during these past couple of months.

I would like to extend my thanks to the Robotics lab, Dr. Shubankar Mishra, Mr. Jyothish Kumar, and Mr. Shriman Keshri for letting us use the 3D printer and for getting the prints done during odd hours. I thank Mr. Subasha Rout for his help with electronics and the mechanical engineering tasks we were involved in. His experience and knowledge with circuits are extraordinary. I take this opportunity to thank Dr. Shuddha Dasgupta for his advice regarding the experiments performed, and also welcome him to NISER, Bhubaneswar.

I would like to thank Mr. Aman Upadhyay, Ms. Adishree M., and Mr. Chinmay Routray for all the cherishable conversations and for bearing my attitude when deadlines were looming over, almost every time.

I thank Mr. Ashish Pandav (one of those lakh guldastas), Mr. Debasish Mallick, Mr. Dukhishyam Mallick, Ms. Mouli Chaudhuri, Mr. Prottay Das, Mr. Sudipta Das, and Ms. Swati Saha for making the lab environment memorable, and I proudly say this, the best amongst all of SPS.

I finally, and I dare not say the least, my parents and sister for the patience and ever-showering love during all the times I hadn't called them.

ABSTRACT

This project involved studying the interaction of radiation and particles with matter. We then briefly describe a few Micro-Pattern Gaseous Detectors, the changes in their design over the years, and finally describe the GEM and the Thick-GEM detector. A Thick-GEM detector was fully constructed and assembled, and this report describes the various details of the fabrication process. The tests involved before we begin characterizing the detector are also described. Finally, some plans for future tests to be conducted are described.

Contents

List of Figures

List of Tables

Chapter 1

Energy Loss of Particles in Matter

A crucial objective in most nuclear or particle physics experiments is the detection of the radiation and particles. It is thus important to look at how different particles and radiation interact with matter. These interactions can be classified into two types based on whether the incident particle is a photon or a charged particle. The subsequent sections go into the details of the same. This project is related to a class of detectors known as gaseous detectors and as the name suggests, they involve working with gases to detect incoming particles based on how it interacts with the gas atoms/molecules. Information like energy and position of an incoming particle can be obtained based on these interactions.

1.1 Interaction of Charged Particles With Matter

A charged particle traversing through matter can be characterized by the following interactions it can undergo with the atoms/molecules of the medium [7]:

1. Inelastic collisions with atomic electrons of the medium
2. Elastic scattering with the nuclei of the medium
3. Emission of Cherenkov radiation
4. Nuclear reactions
5. Bremsstrahlung

As explained in [7], inelastic collisions with electrons of the medium and the incident particle involve the excitation or ionization of these electrons and although the energy lost by the incident particle is not a lot for one such collision, it adds up to a huge number because of the total number of such collisions that usually take place. Elastic collisions with the nuclei of the medium do not take place as often as the inelastic collisions with the electrons of the medium, and these types of collisions do not account for the majority of energy loss of the incident particle. The other three effects also are possible but are less frequent than the first two.

It is useful to calculate the amount of energy lost by an incoming particle as it traverses through a medium, and it was the seminal work of Niels Bohr, Hans Bethe, and Felix Bloch among others that paved the way for these calculations. The information from these calculations formed the foundations based on which we built detectors that can now help us identify the (charged) particle and calculate the energy with which they hit the detector. Although Bohr derived the stopping power (mean energy lost per unit path length) for heavy charged particles using classical arguments, it was Bethe and Bloch that performed the same using quantum mechanics. The derivation by Bohr is explained in Appendix A.

The Bethe-Bloch equation describes the energy loss (through many interactions) that heavy-charged particles like alpha particles undergo while traversing through a medium. The equation is as follows:

$$-\frac{dE}{dx} = 2\pi N_{\mathrm{a}} r_{\mathrm{e}}^2 m_{\mathrm{e}} c^2 \rho \frac{Z}{A} \frac{z^2}{\beta^2} \left[\ln\left(\frac{2m_e \gamma^2 v^2 W_{\max}}{I^2} \right) - 2\beta^2 - \delta - 2\frac{C}{Z} \right] \tag{1.1}$$

here r_e and m_e are the radius and mass of an electron respectively, N_a is the Avogadro's number, I is the mean excitation potential, Z, A, and ρ are the atomic number, atomic weight, and density of the medium respectively, z and v are the charge and velocity of the incident particle respectively, δ and C are the density and shell correction terms respectively and W_{max} is the maximum energy transfer possible in a single collision (obtained from kinematics).

The expressions obtained by Bohr and Bethe-Bloch arise from classical and quantum mechanical frameworks respectively. But it is also to be noted that apart from the correction terms, the final equations have the same dependence on z, Z, A, ρ, and differ in v by one degree. (Here degree means the power of the variable. Eg - degree of x in x^3 is 3.) Bohr's results is pretty accurate considering it was derived for a classical picture.

The density correction term is to deal with the polarisation that the incident particle can bring about in the atoms of the medium along its path. Due to this, the electrons further away from this path will experience a shielding from the true electric field intensity of the incident particle. The Bethe-Bloch equation would break down if the velocity of the incident particle is comparable or lower than the orbital velocity of the bound electrons of the atoms of the medium, this is because the equation assumes that the electrons of the medium are stationary with respect to the incident particle. The shell corrections precisely look into this aspect, it accounts for effects that arise when the velocity of the incident particle is low.

We see that the Bethe-Bloch equation is initially dominated by the β^2 term, so there is a drop in dE/dx as the energy of the incident particle increases. At higher energies, the logarithmic term starts to weigh in, thus increasing dE/dx and ideally should keep on increasing as the energy of the incident particle also increases, but

this rise is canceled due to the density correction term [7].

We mentioned that the incident particle for the Bethe-Bloch equation to apply, has to be a heavy charged particle, and electrons and positrons are light charged particles. This condition exists because the derivation involves assuming that the incident particle remains undeflected as it traverses through the medium. With electrons, we also arrive at the indistinguishability problem when it collides with other electrons of the medium. But one can still modify the Bethe-Bloch equation to obtain an equation for stopping power [7]. Additionally, Bremsstrahlung also has to be factored in to calculate energy loss through the same process.

1.2 Interaction of Photons With Matter

The interaction of photons with matter happens majorly through the Photoelectric effect, the Compton Effect, and the Pair-Production Effect. Depending on the properties like the incident energy of the photon, the cross-sections of each of these processes vary.

The photoelectric effect refers to the emission of electrons when a photon interacts with it. It occurs when the energy of the incident photon is higher but around the magnitude of the ionization energy of the atom. Sometimes the photon can eject an inner shell electron followed by rearrangement of electrons in the atom producing another photon or electron during the process.

Compton effect occurs when the energy of the incident photon is to some extent greater than the ionization energy of the atom. It is the process of transferring some of the energy and momentum to an electron the photon collides with. Similar to Compton scattering, we also have Thomson and Rayleigh scattering. Thomson scattering is the scattering of photons by free electrons, but in the classical limit (low energies). Rayleigh scattering is the scattering of photons by atoms acting as an entity.

The Pair-Production effect is observed when the incident photon is of energy greater than twice the mass of an electron. Pair production often refers to a photon creating an electron-positron pair near a nucleus.

As explained, the above processes come into the picture at different energies of the incident particle, or in more rigorous terms, the cross-sections of the above processes vary with different energies of the incident particle. Figure 1.1 is an example of the same. Note that coherent scattering is another name given to Thomson scattering and incoherent scattering is Compton scattering.

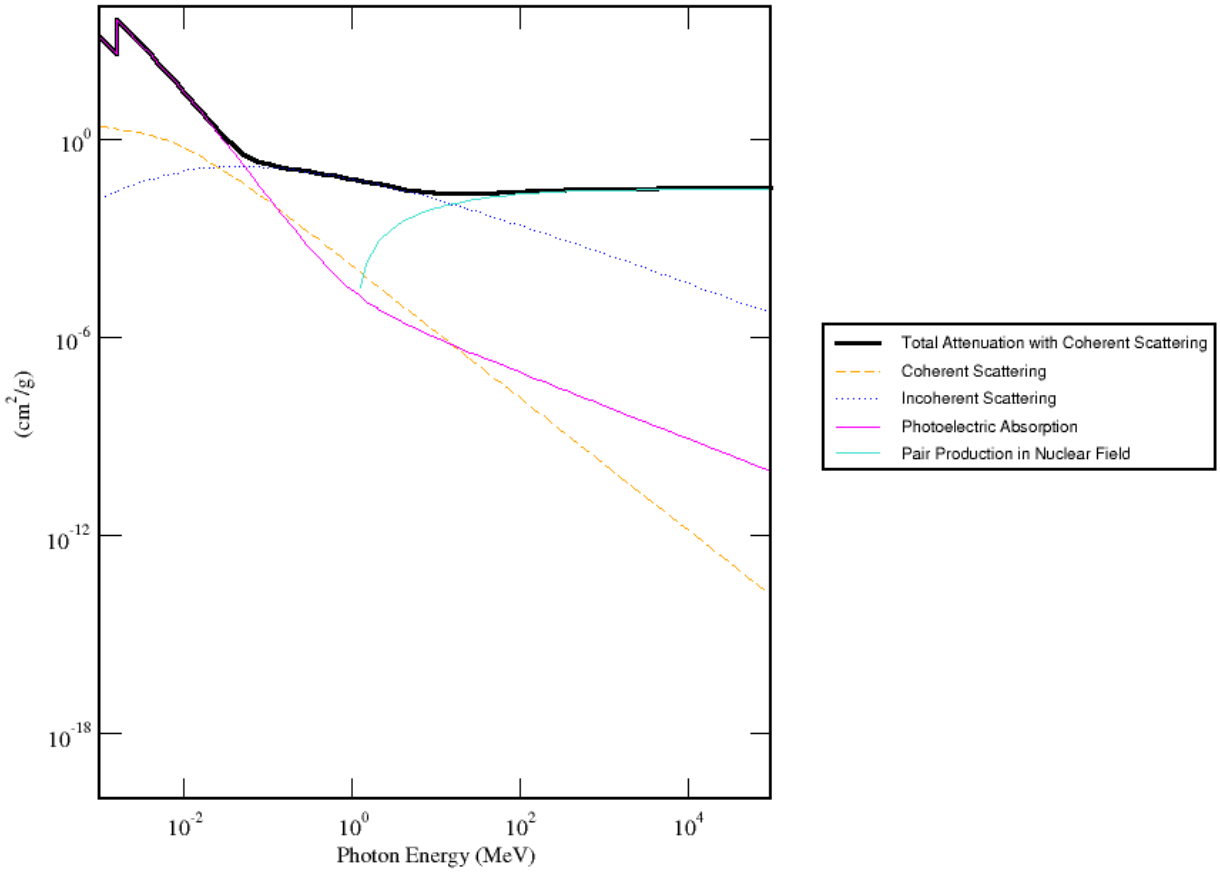

Figure 1.1: Total photon absorption cross-section for Aluminium. Source: National Institute of Standards and Technology.

1.3 Interaction of Neutrons With Matter

Neutrons are particles with no charge and hence are not involved in any electromagnetic interaction with charged particles at the energies we are concerned with. But they can interact with other nuclei through the following processes [7]:

1. Radioactive neutron capture
2. Fission
3. Elastic and inelastic scattering from nuclei
4. Nuclear reactions where the neutron is absorbed into the nucleus and charged particles are emitted.

Chapter 2

Micro-Pattern Gaseous Detectors

It is quite fascinating, how a seemingly-simply process like ionization can lead to a vast range of detector designs, particularly through avalanche processes. The underlying principle in most gaseous detectors in one form or another are electromagnetic interactions. Once an incident ionizing particle enters a gaseous detector, it ionizes and produces one or more primary electrons. External electromagnetic fields present, provide kinetic energy to these electrons accelerate and gain enough energy to create secondary interactions, and produce more ion-electron pairs, thus generating a readable output. There are different innovative designs of gaseous detectors to achieve the above characteristics. In 1968, Georges Charpak invented the Multi-Wire Proportional Counter (MWPC) and this invention set the advent to a plethora of gaseous detectors that followed. We will not go into the details of all the gaseous detectors, but instead offer a brief description of some of the common gaseous detectors. Sections 2.4 and 2.5 will cover the GEM and Thick-GEM detectors in a bit more detail as they pertain to the main topic of this project.

2.1 Multi-Wire Proportional Counter

The MWPC is what one would obtain if multiple proportional chambers are duplicated and combined. It consists of a set of thin, parallel, and equally spaced anode wires between two cathode planes. Negative potentials are applied to the cathode and the anode is grounded. Once an incident ionizing particle ionizes the gas molecules as it traverses through the detector, electron-ion pairs are generated and they start drifting towards the electrode. The electric fields generated through this setup are sufficient to provide enough energy to ionize further electrons and thus generate a readable signal. The cross-sectional schematic diagram of the MWPC is as shown in Figure 2.1.

The MWPC has a good spatial and energy resolution but issues persisted with the rate capability and owing to the slow evacuation of positive ions, a buildup modified the electric fields. But the MWPC gave rise to the advent of detectors based on unique ideas like the drift chamber. Then the drift chamber and the MWPC coalesced to form the Time Projection Chamber.

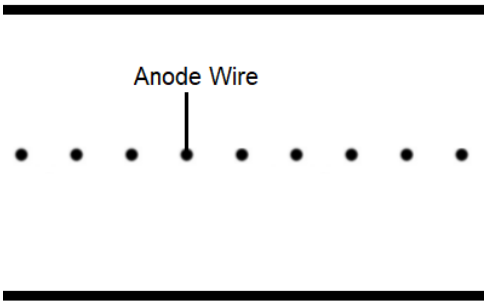

Figure 2.1: A cross-sectional schematic diagram of an MWPC.

2.2 Micro-Strip Gaseous Chamber

The advances made in photo-lithography techniques and microelectronics helped with the creation of the Micro-Strip Gaseous Chamber (MSGC) that offered better rate capabilities compared to the MWPC [6]. The MSGC consists of alternately placed narrow and wide thin metallic strips placed on an insulator. There is also a drift cathode plate on top. The narrow and wide strips are anodes and cathodes respectively and the electric fields around these strips can increase to orders of kV/cm. As mentioned in Ref. [6] and [5], the form of the electric field is such that the ions produced by the avalanche evacuate rapidly, thus crossing the hurdle MWPCs couldn't by providing better rate capabilities.

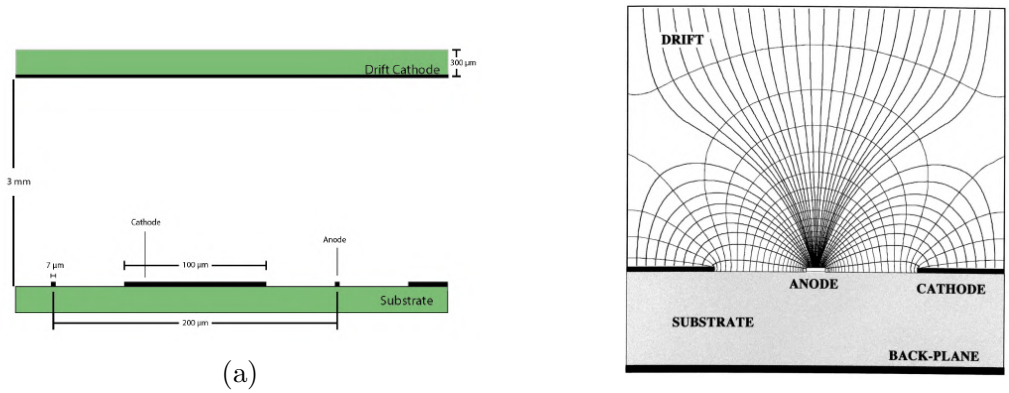

(a) (b)

Figure 2.2: (a) A schematic cross-sectional diagram of the MSGC with typical dimensions. (b) The electric field lines of the MSGC. Source: [11]

One particular disadvantage of MSGCs is charging up effects (in the insulating surface at the bottom). This arises due to the diffusion of electrons and ions generated

during the avalanches. The charges accumulated can result in discharges that can melt the metallic strips. We will see in a later section that with respect to these kinds of issues, how the Thick-GEM detector is a more robust detector than most gaseous detectors.

2.3 Micro Mesh Gaseous Detector

Until now, we have described detectors with wires or strips, the MICRO MEsh GASeous (micromegas) detector on the other hand introduces a mesh in between. In this detector, the gas volume is divided into two by a metallic micro-mesh, but the multiplication region (the region below the mesh, about 50-100μm in height) is very narrow compared to the region above the mesh. There is a drift electrode on top and readout strips on the bottom. The amplification happens around and under the mesh. High electric fields (40–80 kV/cm) are created in the amplification gap by applying a voltage between the grid and the anode [5].

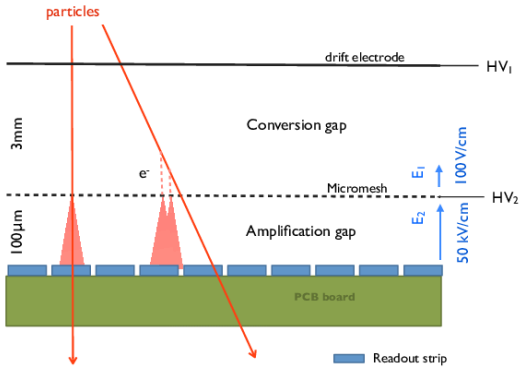

Figure 2.3: Schematic diagram of the micromegas detector. Source: Performances of anode-resistive Micromegas for HL-LHC.

As explained in [6], these detectors offer good spatial resolution and have a fast response owing to the small amplification gap, where the large number of electrons produced, have to travel for a small distance to reach the readout.

2.4 Gas Electron Multipliers

In 1996, Fabio Sauli introduced GEMs [10], which are electron multipliers made from a copper-cladded polymer foil perforated by a high density of holes. The GEM electrode is pierced by a regular array of hourglass-shaped holes and is produced

by certain etching techniques. High voltages are applied on both copper surfaces to provide for a high voltage gradient. The hole shape of the foil is such that there is a dipole-like field (See Figure 2.4b) that can help with a focused electron path at the center and high gains through multiplication because of the high field values in the hole.

The GEM detector is similar in design to the previous detectors. There is a drift electrode above, and readout strips underneath the GEM foil respectively. The usual dimensions and specifications of the detector will be discussed soon.

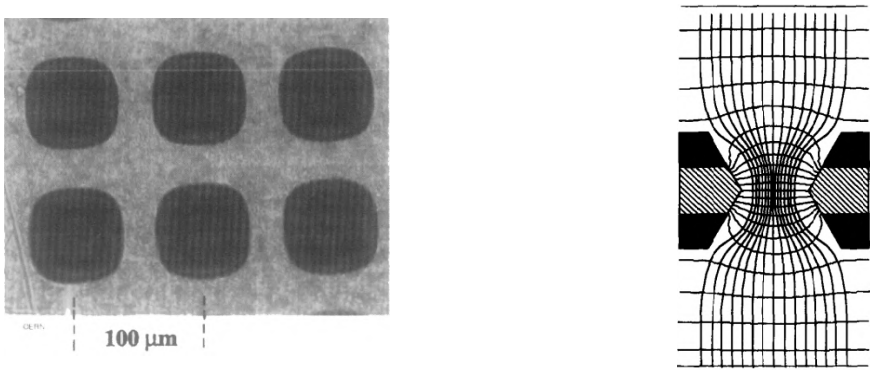

(a) (b)

Figure 2.4: (a) A top view image of the GEM foil. (b) The electric field lines across a GEM hole. Source: [10]

When an ionizing particle passes through, it produces primary charges by ionization, and through drift and diffusion processes, the charges are transported through the gas volume to the amplification region close to the electrodes, and these charges will attain high velocities due to the high electric field and cause further ionizations leading to an avalanche effect. This avalanche process is also called the Townsend avalanche, and is studied in great detail in Ref. [11]. The first Townsend coefficient is a variable that has been extensively studied in gaseous detector physics and represents the number of ion pairs produced per unit length of drift [11]. We will encounter this variable again in Chapter 3. These charges are then collected by the readout pads under the GEM electrode. Separated from the multiplying electrode, the charge collection and readout plane can be patterned at will with strips or pads; usually, they are a set of perpendicular strips to serve as a 2-dimensional readout.

As explained in [11], the GEM detector, with cascaded GEM foils, can reach very high gains, without getting destroyed. This is an important point to make because the previous detectors like the MSGC involved damages when attempts to reach higher gains were made. The readout also can be patterned depending upon the user's needs.

2.5 Thick-Gaseous Electron Multipliers

The Thick-GEM detector is a variant of the GEM detector with dimensions blown up by some factors (details of which we will get to soon), but some structural aspects are different. Thick-GEMs have a cylindrical hole shape, as compared to an hourglass shape in GEMs, which also means the etching process to make these holes are different. Keeping in mind the difficulty in making a precision device such as a GEM foil with its very fine hole diameter along with its small pitch, the Thick-GEM came out to be a device cheaper and easier to manufacture. And the Thick-GEM detector is also very "robust" which means that it has good strength against mechanical force, high electrical fields, ease of handling, etc. As mentioned before, other detectors like the MSGC can get destroyed while operating at high fields, typical GEM electrodes are also sensitive to sparking and can be permanently damaged after a significant discharge, but the etched rim in a Thick-GEM helps reduce edge discharges [3]. To make a GEM electrode one needs high-precision tools to make structures at such dimensions, but the Thick-GEM can be made without such stringent requirements. Figure 2.5 and Table 2.1 gives us a better idea of the difference between both detectors in terms of foil specifications.

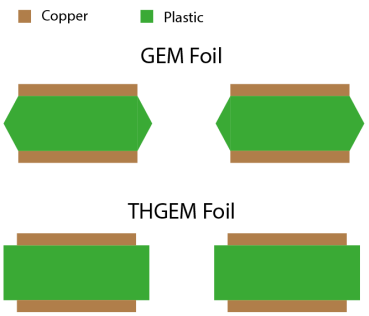

Figure 2.5: Cross-section schematic of the GEM and Thick-GEM holes (Not to scale).

Measurement	GEM	Thick-GEM
Hole Diameter (Inner)	50μm	0.4mm
Hole Diameter (Outer)	70μm	0.6mm
Pitch	150μm	1mm
Thickness	60μm	0.5mm
Electric Field	30-80kV/cm	15-25kV/cm

Table 2.1: Comparison of some specifications between a typical GEM and Thick-GEM foil.

Chapter 3

Fabrication of the Thick-GEM Detector

3.1 Overview

This Chapter will deal with the intricate details of the work done to fabricate and assemble the detector. The main paper that was referred to for guidance is Ref. [13]. It is to be noted here that the fabrication process was a continuation of the work done by me during the sixth-semester project. The contents of Sections 3.2 and 3.3 were performed in the previous project, and everything described thereafter in this Chapter was done as part of the ninth-semester project.

The detector mainly comprises 3 main elements: the drift electrode, the Thick-GEM foil, and the readout pads; all of them placed inside a gas enclosure, with a window on top that is transparent to incoming particles but yet keeping the detector air-tight. The drift electrode is usually a metallic mesh with a voltage to provide a drift field, usually of magnitude 2kV/cm. As the name explains, the drift electrode makes the charges produced under it, attain a drift velocity so they are directed towards the Thick-GEM electrode. The electric field produced in the Thick-GEM holes due to the voltage supplied on both copper surfaces is usually around 30kV/cm. Under the Thick- GEM electrode is the induction gap with an electric field, usually around 1kV/cm. This region helps in directing the electrons to the readout pads where the signal-current is generated, thus giving us a readable output. The entire setup will be in an airtight gas enclosure made with perspex on the sides, Mylar as the top layer (also serving as a window for incoming particles) and the bottom will be a PCB board with readout pads. The detector can be divided into three regions based on the electric field values that will be applied, namely the drift region, Thick-GEM hole region, and the induction region. The same has been labeled in the schematic diagram shown in Figure 3.1. The Thick-GEM foil we are using is 0.25 mm thick, and inner and outer hole diameters of 0.2 mm and 0.3 mm respectively. The pitch between the holes is 0.45 mm. The following components are needed to fully construct the detector:

- Outer air-tight enclosure and top-enclosure

- Readout strips
- Drift electrode
- Electronics

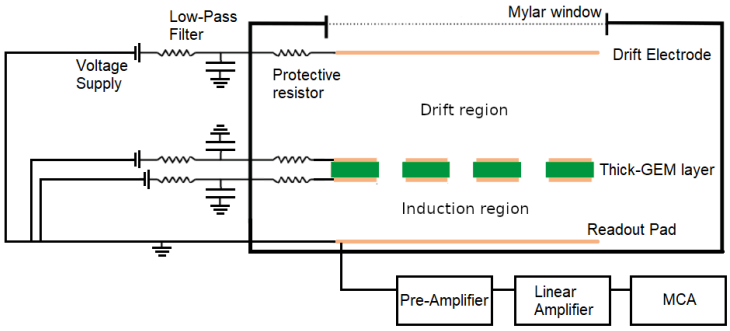

Figure 3.1: A cross-sectional schematic diagram of the detector, along with the electronic circuits used.

The subsequent sections will describe the components and provide details of the manufacturing process, if relevant.

The drift electrode is essentially Aluminium tape pasted on a Mylar sheet (with a contact for a connection to the voltage source). The sheet is held by a Poly-Lactic Acid (PLA) frame (3D-printed) to provide support and keep it flat so it does not bend due to its weight. The dimensions of the working area of the drift electrode is 10×10 cm^2. Under the drift electrode, is the Thick-GEM foil which has three layers, a top copper electrode, a middle FR4 layer, and a bottom copper electrode. The total working area of the Thick-GEM foil is also 10×10 cm^2. The anode then comes under the Thick-GEM foil, which in our case are the readout strips. The Thick-GEM foil and the drift electrode are kept at a height of 2.5 mm and 7.5 mm from the base respectively using nuts. There is thus a gap of 5 mm between the drift electrode and the Thick-GEM foil. Figure 3.1 is a schematic diagram explaining the same.

There are rectangular copper strips provided at the drift electrode and Thick-GEM foil for the voltage connection (See Figure 3.2). The contacts from different layers of the electrode have been connected to other contacts for extension purposes, which will come out of the gas enclosure and can be understood by looking at Figure 3.3. This makes it easier to apply the required voltages to each layer outside the air-tight enclosure.

We finally close everything with an enclosure of height 1.5 cm which will make the entire setup airtight, and we also provide an inlet and an outlet valve for gas flow (See Figure 3.4). The top portion of the enclosure is made of PLA and a Mylar window

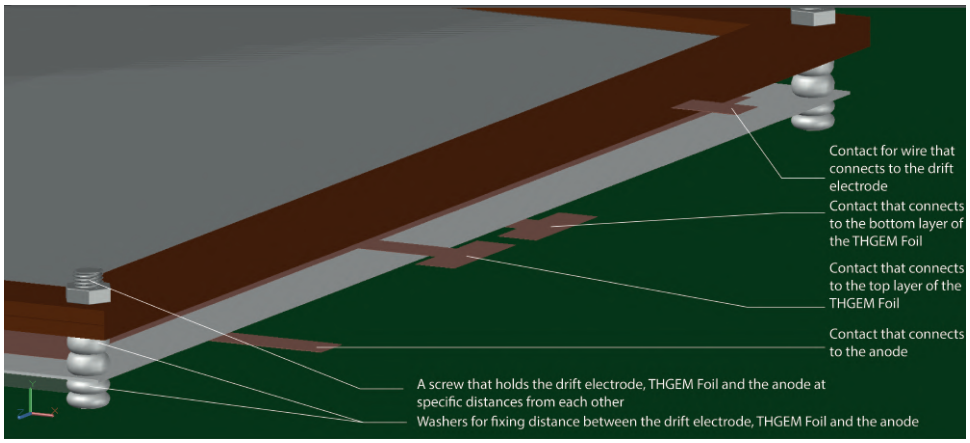

Figure 3.2: Isometric view of the design of the detector made using AutoCAD.

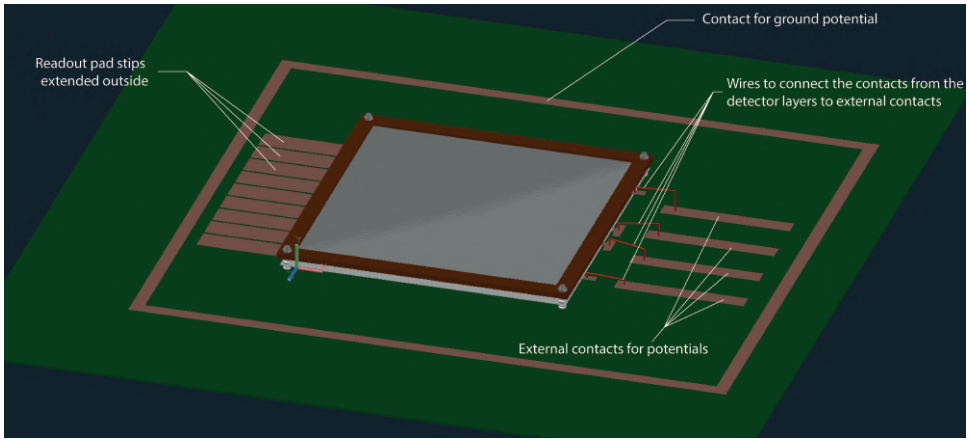

Figure 3.3: Second isometric view of the detector.

(which would serve as a window for incoming particles). Perspex is used for the side walls of the air enclosure.

The contacts for the 4 potentials for the detector will all be connected to a serial 10 MΩ resistor, a 50 Hz low pass filter (using a 2.2 nF capacitor and a 10 MΩ resistor), and then to the power supply, which is a CAEN N1470 High Voltage (HV) supply. The series resistance is added as a protective resistor (against current surges) and the low pass filter is to limit AC voltages that can arise from the voltage supply. We will see that frequencies in voltages can act as a source for noise in a later section. The potentials that will be supplied to the contacts are as shown in Table 3.2.

For the potential values applied, the electric field magnitudes for different regions would correspond to values shown in Table 3.2. These were also the same field values used in Ref. [13]. But there are no universally fixed field values for these regions,

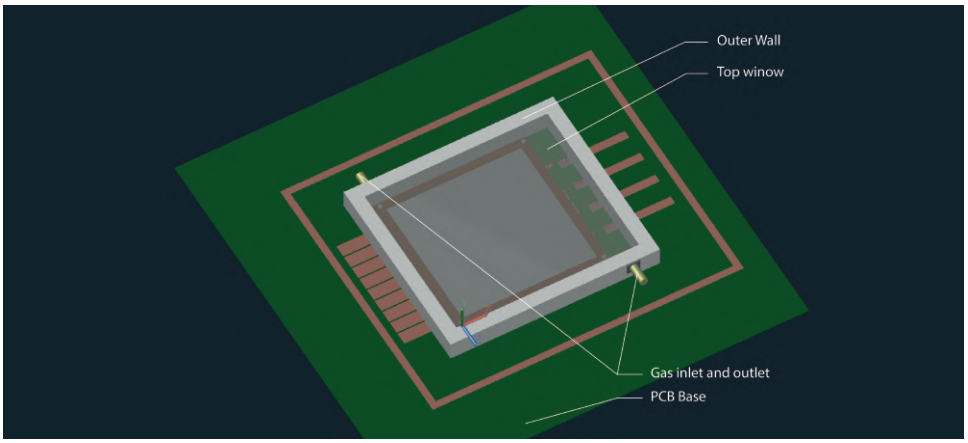

Figure 3.4: Top view of the detector showing the two electrodes and the Thick-GEM Foil.

Surface	Potential (V)
Drift Electrode	-2000
Top layer of Thick-GEM foil	-1500
Bottom layer of Thick-GEM foil	-1000
Anode	Gnd

Table 3.1: Typical potentials that are supplied to each electrode in the detector.

they vary based on the detector specifications and other aspects like materials used, quality of assembly, etc.

Region	Height (mm)	Field (kV/cm)
Drift region	5	1
Thick-GEM hole region	0.25	20
Induction region	2.5	2

Table 3.2: Dimensions and electric field magnitudes for different regions in the detector

The readout strips were connected to the pre-amplifier, a linear amplifier (CAEN Spectroscopy Amplifier M968), a Multi-Channel Analyser (MCA) (Ortec 927 ASPEC MCA), and finally a computer to store the output from the MCA.

3.2 PCB and Readout Strips

Ten readout strips made of conducting material (Copper in our case) were required to be placed under the Thick-GEM electrode. So a Printed Circuit Board (PCB)

board with copper-clad on both sides was taken as the base from which Copper will be etched out, leaving only the readout strips behind.

In order to etch out the unwanted copper, we carried out a displacement reaction using a $FeCl_3$ solution. The corresponding displacement reaction is as follows:

$$FeCl_3 + Cu \rightarrow FeCl_2 + CuCl$$

We prepared a mask using readily available toner ink which acted as a physical barrier, under whose region, the $FeCl_3$ would not react. So after dipping the board in this solution $FeCl_3$ would remove copper wherever the mask was not present. We printed the mask layout on OHP sheets (these are transparent sheets used for Over-Head Printers, from where the name arises) using a laserjet printer. These sheets were then placed at appropriate positions on the PCB board and ironed due to which the toner ink on the sheets was transferred to the PCB board thus completing the masking process. Then an appropriate $FeCl_3$ solution was prepared and the board was placed in the solution and was agitated until all the copper from the desired regions was removed. To then remove the mask, we washed the toner ink with Propanol which removed the ink but not the Copper under it. The board after this etching process is as shown in Figure 3.5.

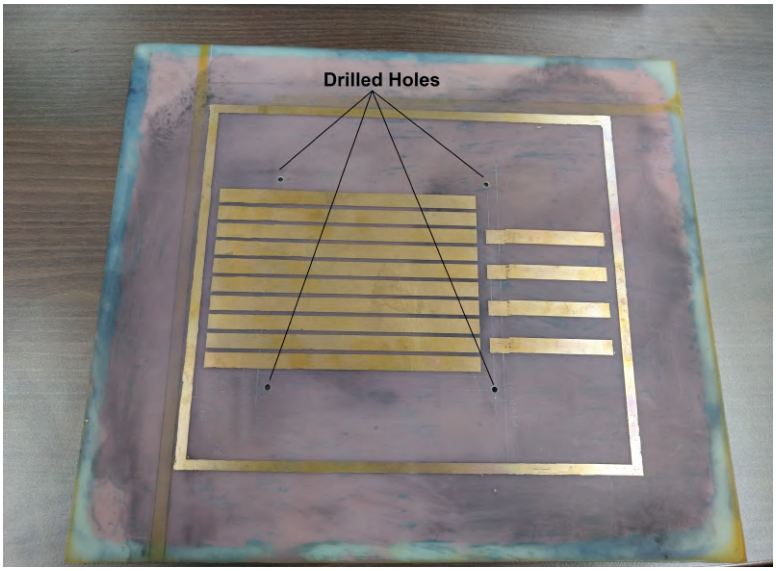

Figure 3.5: The PCB with the readout strips and other terminals after the chemical etching process. Four holes were also drilled which will be used to hold the Thick-GEM foil and the drift electrode.

3.3 Drift Electrode

As mentioned earlier, the drift electrode was made with Aluminium, Mylar, and a frame to hold the Mylar and Aluminium flat and sturdily. The support structure frame is made of PLA and was designed and 3D printed (printed using NISER's Robotics Club's 3D printer). Then a Mylar sheet was stuck on top of the frame to serve as a base for the Aluminium tape to be pasted upon. The voltage supply would be connected to this Aluminium layer with the voltage as mentioned in Table 3.1.

(a) (b)

Figure 3.6: (a) The Perspex frame with the inlet and outlet valves. (b) The rubber layer that will be placed on top of the Perspex layer to act as a seal for the joint.

3.4 Air-Tight Enclosure

The Thick-GEM detector has an inlet and an outlet for gas flow and the remaining volume needs to be airtight. To form a gas-tight container around the anode, foil, and drift electrode, we make four walls using Perspex along with an inlet, and an outlet for the gas flow was built (See Figure 3.7a), with a top enclosure. The interior dimensions were approximately $15.4 \times 14.4 \times 1.5$ cm^3. The top enclosure was made with a 3D printed structure with an open window that was covered with Mylar which would serve as an entry of source particles.[1] The objective was to make a top enclosure that can be opened and sealed if we needed to change components or perform some checks. All components inside this chamber would be in an airtight environment with gas being brought in and flushed out at a constant rate.

Since the side walls were sealed with Araldite, they are never tampered with and do not account for any gas leak. The Mylar sheet that would be placed for the window

[1] Although can be included in a future test, we do not know if PLA would allow particles of our source (5.9keV X-Rays from ^{55}Fe) to pass through, whereas Mylar and Kapton are materials used as a window for irradiated particles to pass through [4].

was pasted and sealed with Araldite. The only source for a gas leak can arise from the top enclosure and motivated by the design of O-ring joints [8] (See Figure 3.8a) that are used in vacuum chambers, we designed an enclosure that when tightened to the Perspex frame with screws, can form an air-tight joint. We experimented with many designs but the final top enclosure has a protruding ridge from the flat surface (See Figures 3.7c, 3.8c). The entire wall was drilled with holes so that screws can go all the way and be able to lock the top enclosure to the Perspex walls. For a good seal, we cut a rubber mat and placed it on top of the Perspex later (See Figure 3.7b). Gas leak tests were also conducted with different materials like thermoplastic elastomers[2], foam, Teflon layers, etc.

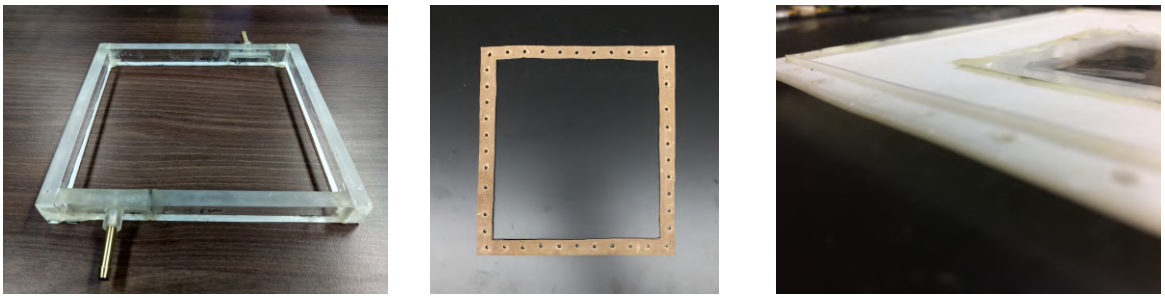

(a) (b) (c)

Figure 3.7: (a) The Perspex frame with the inlet and outlet valves. (b) The rubber layer that will be placed on top of the Perspex layer to act as a seal for the joint. (c) A zoomed-in image of the top enclosure to show the ridge.

We performed a gas leak test, i.e measure the rate at which gas leaks for different pressures for the design that was finalized. We flow some gas inside the detector and then block the inlet and outlet valves leaving the detector with gas inside it, at some initial pressure. We then note the pressure inside it (using a U-tube manometer) at certain intervals of time. The initial designs had performed very badly, losing all air in a matter of seconds. The manometer does not provide us with information about where the leak is occurring. We then gauged the amount of gas leaking and regions from where it is leaking by placing the setup (without the foil, drift electrode, and electronics, but with the gas flow) underwater. This gave rise to bubbles from locations where the setup has gaps or holes. When we arrived at a setup where there were no bubbles visible, the pressure drop (measured with the manometer) was still not satisfactory. Dipping the setup in soap water, instead of water, further provided us with additional areas of improvement that were needed to make the setup leak-proof. After these changes, the plot of pressure inside the container vs time was plotted and is shown in Figure 3.9b, but after tightening the screws of the joint between

[2]a material that increases in tack when heat is applied; such materials used in glue-guns

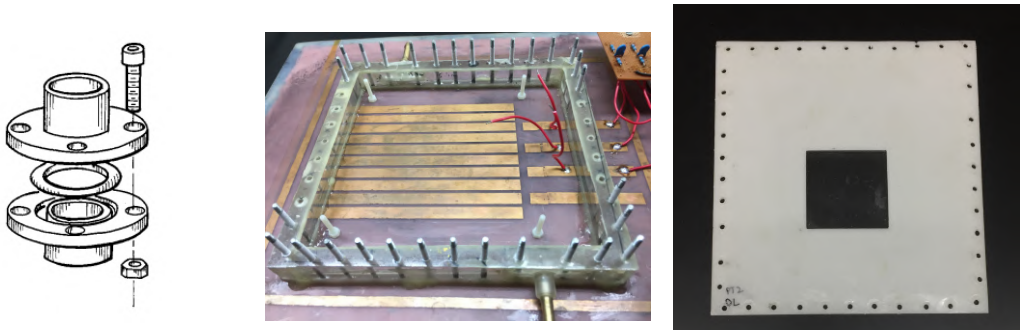

(a) (b) (c)

Figure 3.8: (a) An O-ring sealed vacuum connection (Source: [8]). (b) An image of the detector after the placement of the Perspex walls and installation of screws taped with Teflon to prevent gas leaks. (c) Image of the top enclosure.

the Perspex frame and top enclosure, the subsequent gas leak test (See Figure 3.9b) which was performed for a larger period) gave a lesser leak rate.

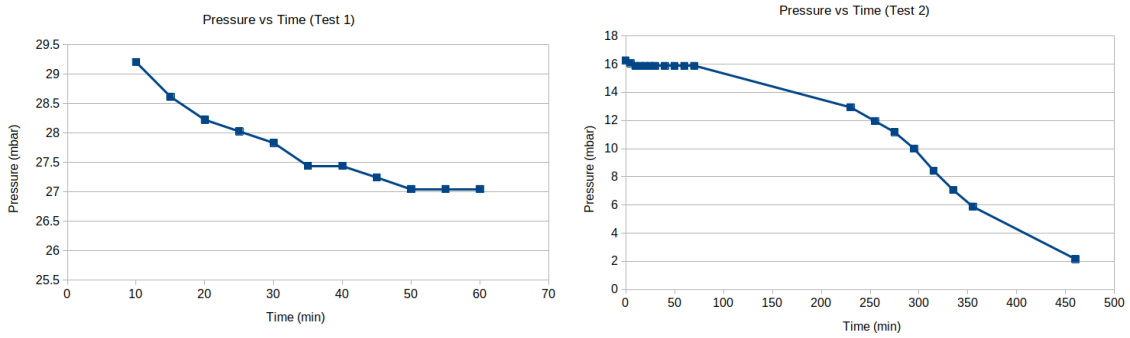

(a) (b)

Figure 3.9: Gas leak rate for the (a) first attempt and (b) second attempt (tighter joint).

Based on a couple of gas-leak tests, we were able to obtain an average leak rate of about 2.2 mbar/hour. For comparison, a recent presentation by a group from Punjab University that assembled and sent GEM detectors to be used in the CMS experiment, showed gas leak rates of (0.4-4.2) mbar/hour. Since the leak rate of the detector we built falls well inside this range, we thus have successfully fabricated an enclosure with an acceptable gas leak rate.

3.5 Assembly in a Clean Room

The hole size of the Thick-GEM foil prevents us from leaving it open to the air, it rather requires to be handled in a clean room so that no dust particles interfere. If any dust particles are present in the detector, then the efficiency of the detector can drop, sometimes even leading to electrical discharges at such high voltages. Before placing the Thick-GEM foil, the detector was cleaned and handled in a class-100[3] clean room at NISER. Furthermore, the Thick-GEM foils were opened and placed inside the cleaned setup, inside a laminar airflow table, which as the name suggests, has a laminar airflow inside the chamber.

After the Thick-GEM foil was placed, the drift electrode was placed above it and the required HV supply connections were soldered and the whole setup was closed with the top enclosure, thus making the setup airtight. The design of the detector is such that the HV supply can be made outside without having to open the setup every time we have to change the supply points.

An Ar+CO_2 (70%-30% ratio respectively) was used as the gas mixture, and the setup was flushed with this gas mixture for a few days until the detector was tested.

3.6 Gas Selection and Quenching Gases

The Thick-GEM detector is a gaseous detector, but we never discussed what gasses to use or why use them. For the selection of the gas, one needs to keep in mind that the gaseous constituents should not have a high electron affinity to attract the electron before it even begins the avalanche effect. Keeping in mind the physical conditions required to keep the substance in its gaseous state, noble gases are good choices. After ejecting an electron one might argue that the noble gas atom attains halogen configuration, but by the time it pulls the electron, the electron under the external electric field would have begun subsequent collisions. There are other favorable reasons for noble gases. Nobles gases are inert, and that is also why they are a good choice, and what is meant by this is that they are chemically inert so they do not react with the detector materials. They also do not catch fire easily and this is relevant because sparking is something very likely to happen in such detectors. We do not need gases that catch fire inside during the experiment.

We also add other relatively inert gases like CO_2 and CH_4 to the gas, and they are called quenching gas. This is done to reduce the gain, as a very high gain can also lead to a higher discharge probability. Higher discharge probability means higher chances for the Thick-GEM foil to get destroyed. These gases are electronegative, so at times

[3]To offer some perspective, a class 100 cleanroom contains a maximum of 832 particles greater than a size of 1μm.

they absorb the electron from an ionized atom preventing further amplification.

3.7 Electronics

The protective circuits for the HV supply were mentioned before. Additionally, we have the equipment to obtain, shape, and amplify the signal from the readout strips. This section describes the various components and the subsequent electronic circuits/connections. The train of electronics from the readout strips is the pre-amplifier, amplifier, and MCA.

3.7.1 Pre-amplifier

The readout strips are first connected to the pre-amplifier and we used an Ortec 142 IH charge-sensitive pre-amplifier (preamp) [9]. The primary function of a preamp is to extract the signal (which in our case, are charges that originate due to primary and secondary ionizations) without degrading the signal-to-noise ratio. This is usually why the preamp is placed close to the detector, so that the characteristics of the signal are not disrupted by factors like capacitance changes by cabling, radio-frequency pickup, etc. A charge-sensitive preamp is used generally for energy spectroscopy, and these preamps can measure the quantity of charge and time of arrival. A preamp would consist of an operational amplifier with a feedback capacitor, which acts as a charge integration circuit, thus converting the number of charges to a voltage value. The amplitude of the output is proportional to the quantity of charge.

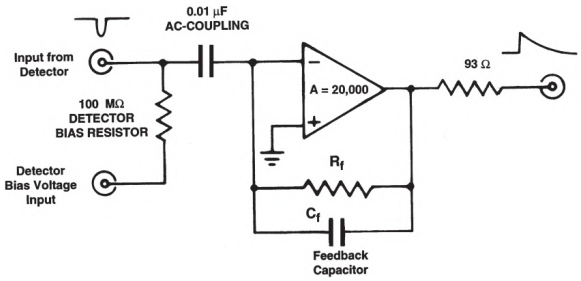

Figure 3.10: A circuit diagram of a typical charge-sensitive preamp. This figure shows how a typical input pulse and output look like. Source: [9]

3.7.2 Spectroscopic Amplifier

The CAEN N968 Spectroscopy Amplifier [12] that was used in the experiment has a variety of functions like amplification, shaping, pile-up rejection, pole-zero cancel-

lation, and baseline restoration. The output of the preamp will be connected to the spectroscopy amplifier for further pulse processing.

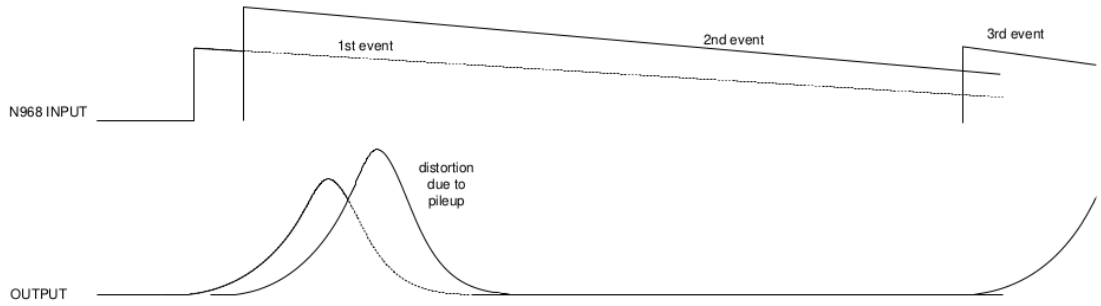

Figure 3.11: A schematic diagram of the input pulse to the amplifier and the output pulse. The inter. We see that the output pulse has been shaped, which is done through a shaping circuit. Source: [12]

The shaping is done through a CR-RC-shaping circuit, and for pedagogical reasons we describe a simple CR-RC-shaping circuit.

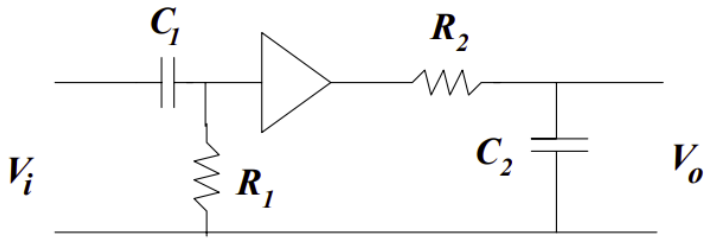

Figure 3.12: The schematic diagram of a typical shaping circuit. Source: [2]

The output of the shaping circuit looks like the output of the amplifier as shown in Figure 3.11. Additional shaping can be done by varying the time constants of the RC/CR circuits. Figure 3.13 conveys the same.

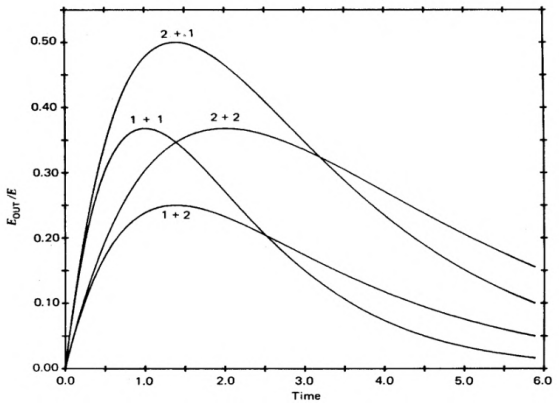

Figure 3.13: The outputs of a CR-RC shaping circuit to a step voltage. Curves are shown for several different combinations of time constants and are labeled as (time constant of CR circuit + time constant of RC circuit). Source: [2]

3.7.3 Multi-Channel Analyser

The MCA is the final piece of equipment we use to process the signal before the information is sent to a computer. The MCA is a device that takes in the shaped and amplified pulse from the amplifier and digitizes it, which means it converts analog information to digital information. We use an Ortec 927 ASPEC MCA for the experiment.

Chapter 4

Testing the Thick-GEM detector

4.1 Preliminary Tests

Before we place a source and start performing any experiments, we need to test for any electrical discharges while increasing the voltage supply slowly. The CAEN HV supply has an inbuilt device to measure the current flowing through the circuit, and the least count can go up to 0.05μA. To prevent the foil from getting damaged from sparks, we set a limit of 20μA on the CAEN HV module, and if a current greater than this value flows (which can arise if there are electrical discharges), the supply automatically switches off. These tests were carried out in two stages:

1. We first increase only the voltages on the Thick-GEM layers in steps of 20V until we reach -1500V and -1000V for the upper and lower layer of the Thick-GEM foil respectively. We observed no current greater than 0.30μA.

2. We then increase the voltages on the Thick-GEM layers and the drift electrode until we reach -2000V, -1500V, and -1000V for the drift, upper Thick-GEM layer, and lower Thick-GEM layer respectively. We observed no current greater than 0.30μA.

4.2 Measuring the Energy Spectrum of ^{55}Fe Source

Once the required components and circuits that are needed to start taking data are in place (See Figure 3.1 for a schematic diagram of the components needed), we placed a ^{55}Fe Source [1] that produces X-Rays of energy 5.9keV, to which we observed no spectrum. We also got no desired output for a Strontium β source, thus eliminating concerns regarding the activity of the ^{55}Fe source that was used.

A secondary setup we often used is to connect the detector output to the preamp and the output of the preamp to an Oscilloscope (Teledyne Wavesurfer 510) to see if we get an output that a preamp gives when there is a signal (This typical output

[1]The ^{55}Fe source produces X-Rays of energy 5.9keV. This characteristic X-Ray arises because ^{55}Fe converts to ^{55}Mn through electron capture, which in turn leads to a re-arrangement of electrons giving rise through these X-Rays.

having a very short rise time and a long decay tail, is as shown in Figure 3.10). This setup was used for the rest of the experiments mentioned in this Chapter, unless mentioned otherwise.

4.3 Components Check

Given that there are no issues from the leak-proof setup and the source, we performed ablative tests with the help of a pulse generator from Agilent (81110A) to see if any of the electronic components we were using was faulty:

1. The oscilloscope was not found to be faulty after the same square wave pulse that was generated from the pulse generator was seen on the oscilloscope too.

2. The preamp has an additional connection called the test input, where one can provide a test pulse for calibration and this connection can also be used for testing/additional calculations. But according to the manual [9], the test pulse that goes into the test input connection should have a rise time of around 20-40ns and a decay time of 200-400μs. The same was achieved using an RC-shaping circuit and appropriate characteristics of a square wave from the test pulse generator. The results of this test indicated that the preamp has no faults. See Figures 4.1, 4.2 and 4.2.

3. With the same circuit and settings as above, we connected the oscilloscope to the spectroscopy amplifier, which was connected to the preamp. The output on the oscilloscope from the amplifier was Gaussian-like which implies that the spectroscopy amplifier too is working as expected.

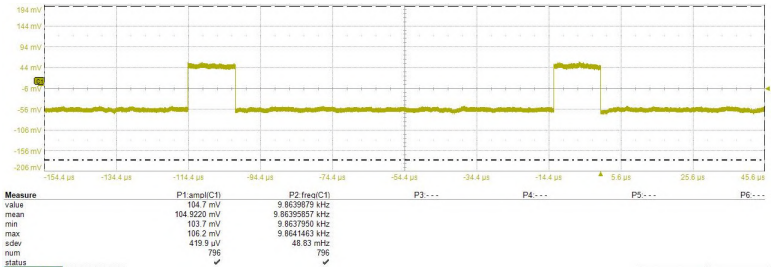

Figure 4.1: The square pulse generated by the pulse generator.

Now that the electronic components were found to have no faults, we cornered the problem to the detector or noise [2], or both. The pursuit from here is to reduce noise levels or increase the effective gain of the detector.

[2]Noise can be a reason for not observing the expected output from the preamp because there is a possibility that the amplitude of the signal is lesser than that of noise

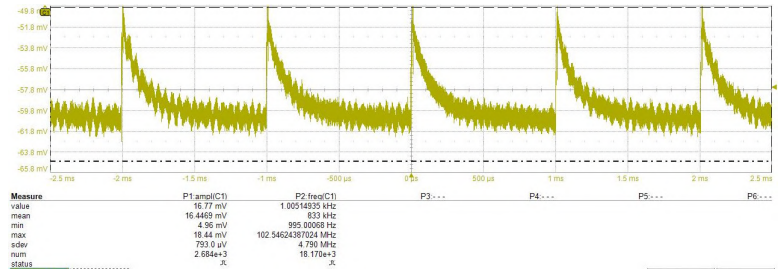

Figure 4.2: The square pulse after being shaped by the RC-shaping circuit.

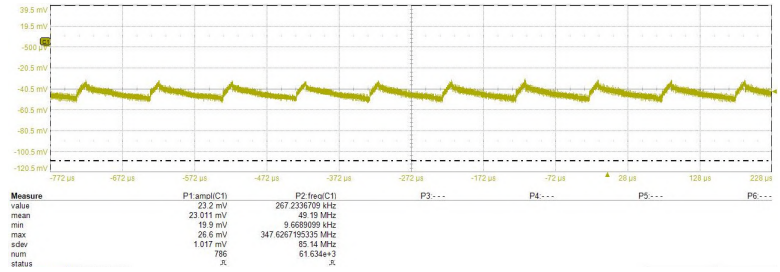

Figure 4.3: The preamp output for the the input pulse shown in Figure 4.2.

4.4 Attempts to Reduce Noise and Increase Signal Amplitude

It was also noticed that switching off the room lights affected the output from the preamp, so a Faraday's cage was built to reduce the effect of stray electromagnetic radiations on the detector output. See Figures 4.4a and 4.4b. The amplitude of the noise from the preamp was around 200mV before placing the detector in a Faraday's cage, and around 3mV after using the cage. Reduction in noise from these stray radiations still did not help in giving a signal.

We were previously using an Ar-CO_2 (70%-30%) mixture. Changing the gas to an Ar CO_2 (80%-20%) mixture (lesser amounts of quenching gas, and thus greater amplification (and possible sparks)) did not help.

In an attempt to increase the amplification by increasing the electric field in the Thick-GEM foil and thus the signal amplitude, we observed signals at electric fields higher than 3kV/cm, 26kV/cm, and 4kV/cm in the induction, Thick-GEM hole and drift regions respectively. Figure 4.5 shows the oscilloscope output of the preamp with an ^{55}Fe source, which is promising, but we also observed the same without the source. Another observation is that the signal amplitude is in the order of volts, which means the number of charges going into the preamp from the readout is too high. We conjectured that the source of this signal was cosmogenic backgrounds like muons (usually of the order of GeVs). Two arguments can disprove this conjecture:

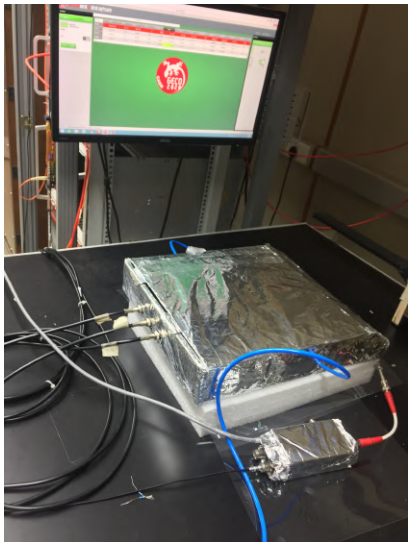

(a)

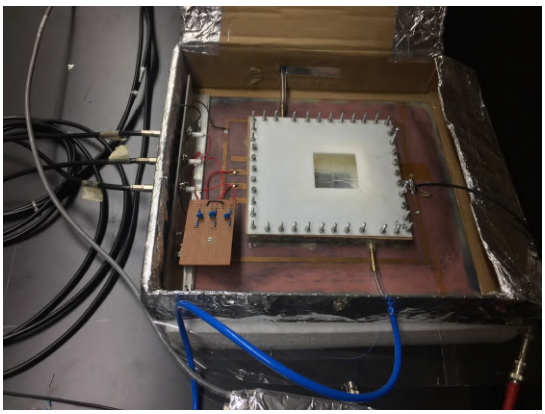

(b)

Figure 4.4: (a) An image of the detector inside the Faraday's cage. (b) An view of the detector inside the Faraday's cage.

- The rate of muons hitting the surface of the Earth is around 10,000 counts/(m^2.min)[3] which corresponds to about 1 count/cm^2min. The rate at we which we were observing the pulses, were around 6 count/cm^2min.
- Even if we assume that these pulses were being produced due to cosmogenic muons, which means that the detector is working, why is the source almost invisible to the detector output (no difference in the pulse count irrespective of the source being placed or not)?

4.4.1 Calibrating the Voltage Range From the Pre-amplifier

With a rough calculation, we can find out the voltage range in which we should be looking for the signal, on the oscilloscope. By voltage range of the signal, we mean the voltage range of the preamp output for the signal. Doing this exercise would give us an idea of how much noise we should reduce or by what factor should the signal be amplified.

We connected the pulse generator to the test input of the preamp and observed the output of the preamp on an oscilloscope. For a square wave pulse of height 50mV, width 60μs and frequency 500μs, a preamp output with pulses of around the same amplitude was obtained. The feedback capacitor in the preamp is what governs the

[3]Source: The Berkeley Lab Cosmic Ray Telescope Project

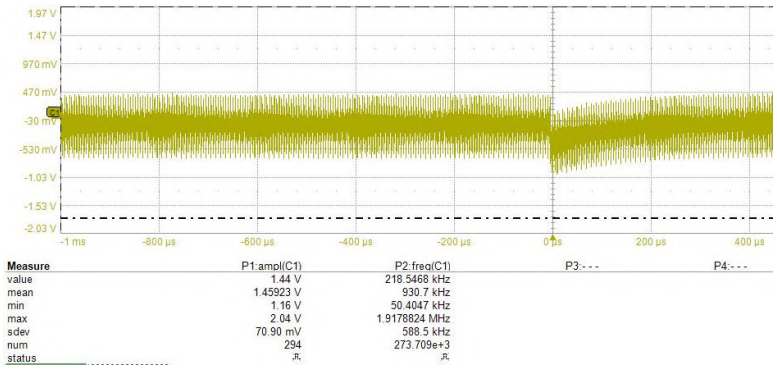

Figure 4.5: The preamp output of the detector with source placed.

height of the output pulse and the voltage is given by $\frac{Q}{C_f}$, where C_f is the capacitance of the feedback capacitor. So we have the following:

$$50mV = \frac{Q}{1pF} \implies Q = 50fC$$

This means that an input charge pulse of 50fC to the preamp, would give us an output of height 50mV. (4.1)

We now try and calculate the number of expected charges from the detector after amplification for Argon-CO_2 (70%-30%) mixture and 30kV/cm field in the Thick-GEM hole region. For the ^{55}Fe source that produces X-Rays of energy 5.9keV, and the mean ionisation energy values (W) for Argon and CO_2 are 25eV and 34eV respectively[4]. The average number of primary electrons produced by an X-Ray is $5.9\text{keV} \times \left(\frac{\%(\text{Ar})}{\text{W(Ar)}} + \frac{\%(\text{CO2})}{\text{W}(CO_2)}\right) = 207.7$ [1]. A more rigorous calculation can be found in Ref. [5].

For a field of 30kV/cm in the Thick-GEM hole region in Ar-CO_2 (70%-30%) mixture, from Figure 4.6, we expect a gain of around 200 (but only if the foil was 1 cm thick). But assuming Townsend coefficient varies linearly for different thicknesses, we expect a gain of the order of 10. Although the value might be approximate for that field, we can always vary the supplied voltage by around 1-2kV/cm to achieve a similar value.

Factoring in this information, along with a number of primary ionizations, we can expect an average of 2200 electrons generated from one X-Ray, i.e in one pulse. This corresponds to 0.3fC of charge reaching the readout strips (∼6250 electrons

[4]Note that the ionisation energies of Argon and CO_2 are higher than those given in sources like National Institute of Standards and Technology. Why is it so?

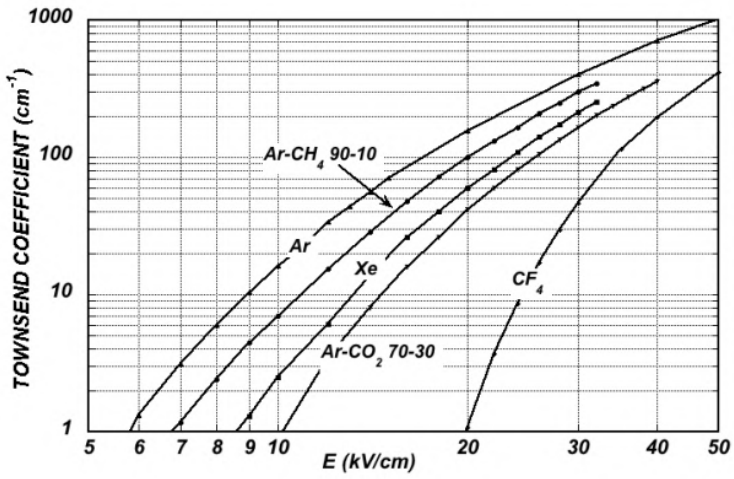

Figure 4.6: Computed first Townsend coefficient as a function of the electric field in several gases at NTP. Source [14]

correspond to 1fC). It turns out that the expected amplitude of signal we expect from the preamp is of the order of 1mV, whereas we are currently getting a noise amplitude 3mV only from the preamp, which has to be reduced.

The 3mV noise is for the setup corresponding to one shown in Figure 4.7a. We then performed another test to see if the detector has some intrinsic noise using the circuit as shown in Figure 4.7b. We observed the noise of amplitude ∼200mV, which is again too high for the signal we are expecting, thus establishing a serious need to find ways to reduce noise or increase the gain of the detector.

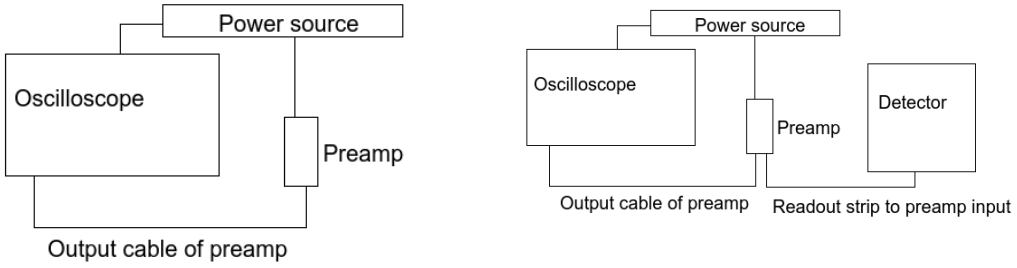

(a) (b)

Figure 4.7: The schematic circuit diagram to measure noise from (a) only the preamp (b) the preamp connected to readout strips of the detector but note that no connections from the high voltage supply were connected.

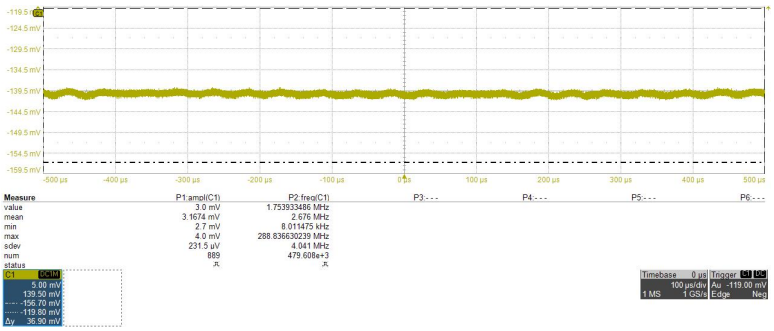

Figure 4.8: The output of the preamp with no connections (See Figure 4.7a for the full circuit).

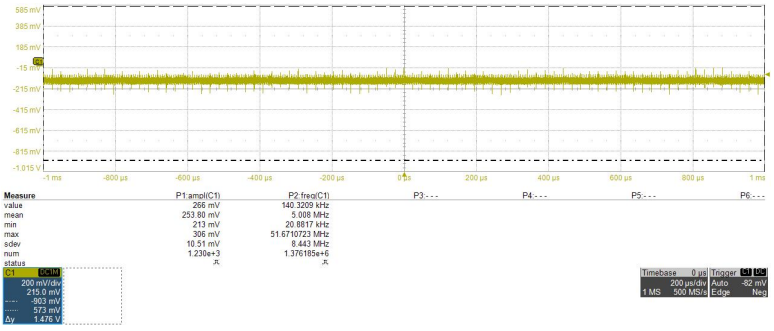

Figure 4.9: The output of the preamp with the readout strip connected (See Figure 4.7b for the full circuit).

Chapter 5

Subsequent Testing

As explained in the previous chapter, we believe that the signal from the ^{55}Fe source is low (in amplitude) compared to the noises we are observing. And as described before, we can proceed further by either reducing the noise or increasing the signal amplitude (by increasing the effective gain of the detector).

5.1 Increasing Signal Amplitude

We can either increase the signal amplitude either by increasing the effective gain of the detector or by amplifying the signal through an appropriate electronic circuit. But the later method also can amplify noise. For now, we focus on the former.

We have only Thick-GEMs of only one configuration (different specifications give different gains). The remaining ways to increase the gain of the detector is through increasing the electric field, or by changing the gas mixtures. Until now, we have tried three different gas mixtures: Ar-CO_2 (70%-30%), Ar-CO_2 (80%-20%), and Ar-CH_4 (90%-10%), and we went up to high fields too, all giving no observable signal from the ^{55}Fe source. We thus have to try finding higher optimum potentials to supply to maximize the gain.

We can also use multiple Thick-GEM foils to increase the gain of the detector. This is done by stacking multiple foils one above the other, with the readout and drift electrode at the bottom and top, respectively, as usual.

There are also more complicated effects that can be studied later on. For example, variation of gain in different sections of the detector, variation of gain for different gas flow rates, and effect of solder (that was added to connect the Thick-GEM layers and drift electrodes to the HV supply) on the gain.

5.2 Reducing Noise

One can observe an outer rectangular copper strip provided in Figure 3.5. This connection was made to provide points for ground connections. All grounds were made common using this strip, including the HV supply ground and the connection from the readout strip. But with a signal containing charges of the order of fCs, a

disturbance in the ground[1] can affect the signal and induce noise. For this reason, we need to build a separate ground point using a large metallic plate, or a very long and thick wire bundle so that it can act as a secondary ground, and given that we know there would not be disturbances from other appliances in the building, this would serve as a stable ground for us. The next step we can take in reducing noise levels is by connecting the ground of the wire from the readout strips (that would transmit the signal to the preamp) to this ground that we would build.

Another interesting problem we had encountered is the observation of large signals with and without the presence of the ^{55}Fe source (See Section 4.4). To figure out the source of these large pulses, there are multiple directions to look at. One important point to note is that we observed these pulses only at higher fields in the detector.

The drift electrode was made using Aluminium tape which is about 5 cm wide. Since the working area of the drift electrode is 10×10 cm^2, we needed to use the tape twice to cover the entire area. The line where this joint is made, would have an edge, around which the electric field would be huge and can act as a source for ionizations. We are planning on covering this edge using a thin Kapton tape to prevent such effects.

The Thick-GEM holes were made using a mechanical drill, unlike a chemical etching process for GEM holes. This allows the possibility of sharp cuts or protrusions in the copper layers, thus again acting as a source for ionizations. We would be doing a spark test by supplying voltage across the foil in the open air and observing if there are any sparks (by visual and auditory inspection) being generated that the CAEN HV module could not pick up. Sparks would come about like a flash to the visible eye, and also makes a distinct noise, which can be picked up by human ears.

[1]This ground is the same one used for all ground connections in the building. Thus other appliances connected to this ground can alter the ground levels.

Appendix A

Bohr's Derivation of Energy Loss of Heavy Particles in Matter

Bohr derived the energy loss that an incident particle would experience when it traverses through some material medium. Let us say the incident particle has charge Ze, mass M and is traveling at a velocity v. The mass of an electron is labeled as m_e.

There are two important assumptions that Bohr makes:

1. M is large enough (M >> m_e) that it does not deviate from its path as it goes through the material.

2. The velocity of the incident particle, v, is much greater than that of the velocity of the bound electrons of the atoms in the medium. This assumption is made so that we further safely assume that these bound electrons are stationary with respect to the incident particle.

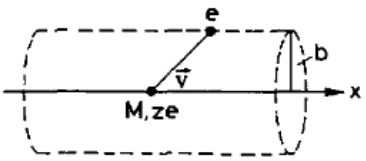

Figure A.1: Schematic diagram of the collision of the incident particle and an electron bound to the atoms of the material. Source: [7]

We now calculate the impulse imparted on an electron at some distance from the incident particle. The distance between these two particles along the z-direction is b, and can be seen in Figure A.1.

$$I = \int F dt = e \int E dt = e \int E \frac{dt}{dx} dx = e \int E \frac{dx}{v} = \frac{e}{v} \int E_{\perp} dx$$

where E is the total electric field of the incident particle and $E_{\perp}$is the perpendicular component. We do not have the parallel component ($E_{\parallel}$) because the values

of $e\int_{-\infty}^{c} E_{\parallel}dx$ and $e\int_{c}^{\infty} E_{\parallel}dx$ are equal and opposite in magnitude. Here c is the x-coordinate of the electron.

Considering an infinitely long cylinder of radius b, with the central axis along the incident particle trajectory. Using Gauss's Law, we get:

$$\int E_{\perp}2\pi b dx = 4\pi ze \implies \int E_{\perp}dx = \frac{2ze}{b} \implies I = \frac{2ze^2}{bv}$$

Thus the energy gained by the electron, given by $\frac{I^2}{2m_e}$ is:

$$\Delta E(b) = \frac{2z^2e^4}{m_e v^2 b^2} \tag{A.1}$$

For N_e being the density of electrons in the medium, the incident particle loses energy to electrons present at a perpendicular distance between b to b + db in a thickness dx given by:

$$-dE(b) = \Delta E(b) N_e dV = \frac{4\pi z^2 e^4}{m_e v^2} N_c \frac{db}{b} dx \implies -\frac{dE}{dx} = \frac{4\pi z^2 e^4 n}{mv^2} \ln \frac{b_{\max}}{b_{\min}}$$

Instead of integrating the above quantity from $b_{min} = 0$ to $b_{max} = \infty$ is a wrong direction to proceed in. This is because, for very large b, the collisions do not occur instantly, thus making the impulse calculations invalid. Additionally, the above equation becomes infinite after setting $b_{min} = 0$.

To obtain the lower limits of the integration b_{min}, we consider the maximum energy transfer possible in a head-on collision. This corresponds to the electron obtaining energy of $\frac{1}{2}m_e(2v)^2$, which can be derived from the kinematic calculations of elastic collisions between a massive particle and a particle with much lower mass. When relativity is taken into account, the value has to be changed to $2\gamma^2 mv^2$, where $\frac{v}{c}$ and $\gamma = \frac{1}{\sqrt{1-\beta^2}}$. Plugging this loss in energy in Equation A.1, we get:

$$b_{min} = \frac{ze^2}{\gamma m_e v^2}$$

To calculate the value of b_{max}, we consider the orbital frequency ν of the bound electrons in the medium. As explained in [7], the impulse transfer should happen in a short time compared to the time period of the bound electron, $\frac{1}{\nu}$. For our collisions, the typical interaction time is given by $t = \frac{b}{v}$, which after accounting for relativity, becomes $\frac{b}{\gamma v}$, so that

$$\frac{b}{\gamma v} \leq \tau = \frac{1}{\bar{\nu}}$$

Considering that there are several bound electrons with different frequencies, we have replaced ν with the mean frequency, $\overline{\nu}$.

Thus, substituting b_{max} and b_{min}, we get the Bohr's classical formula:

$$-\frac{dE}{dx} = \frac{4\pi z^2 e^4}{m_e v^2} N_e \ln \frac{\gamma^2 m v^3}{z e^2 \overline{\nu}} \tag{A.2}$$

Bibliography

[1] Tutor L. Benussi. *GEM detector construction and characterization*. INFN, Frascati, Italy, Oct. 2015. URL: https://agenda.infn.it/event/9123/contributions/77376/attachments/56136/66279/EDIT2015Benussi.pdf.

[2] Andrew Boston. *Pulse Processing: Pulse Shaping*. URL: https://ns.ph.liv.ac.uk/~ajb/ukgs_nis/pre-course-material/lec2-03.pdf.

[3] A. Breskin et al. "A concise review on THGEM detectors". In: *Nuclear Instruments and Methods in Physics Research Section A: Accelerators, Spectrometers, Detectors and Associated Equipment* 598.1 (2009). Instrumentation for Colliding Beam Physics, pp. 107–111. ISSN: 0168-9002. DOI: https://doi.org/10.1016/j.nima.2008.08.062. URL: https://www.sciencedirect.com/science/article/pii/S0168900208012047.

[4] S Bressler et al. "Recent advances with THGEM detectors". In: *Journal of Instrumentation* 8.12 (Dec. 2013), pp. C12012–C12012. ISSN: 1748-0221. DOI: 10.1088/1748-0221/8/12/c12012. URL: http://dx.doi.org/10.1088/1748-0221/8/12/C12012.

[5] M.A. Chefdeville. "Development of micromegas-like gaseous detectors using a pixel readout chip as collecting anode". Undefined. PhD thesis. University of Amsterdam, Jan. 2009. ISBN: not assigned.

[6] Theopisti Dafni. "A Search for Solar Axions with the MICROMEGAS Detector in CAST". PhD thesis. Darmstadt, Tech. U., Oct. 2008.

[7] William R. Leo. *Techniques for Nuclear and Particle Physics Experiments: A How-to Approach*. 2nd. Springer, 1994. ISBN: 3540572805,9783540572800.

[8] John H. Moore et al. *Building Scientific Apparatus*. 4th ed. Cambridge University Press, 2009. ISBN: 0521878586,9780521878586.

[9] *Preamplifier Introduction*. URL: https://www.ortec-online.com/-/media/ametekortec/other/preamplifier-introduction.pdf.

[10] F. Sauli. "GEM: A new concept for electron amplification in gas detectors". In: *Nuclear Instruments and Methods in Physics Research Section A: Accelerators, Spectrometers, Detectors and Associated Equipment* 386.2 (1997), pp. 531–534. ISSN: 0168-9002. DOI: https://doi.org/10.1016/S0168-9002(96)01172-2. URL: https://www.sciencedirect.com/science/article/pii/S0168900296011722.

[11] Fabio Sauli. *Gaseous Radiation Detectors: Fundamentals and Applications*. Cambridge Monographs on Particle Physics, Nuclear Physics and Cosmology. Cambridge University Press, 2014. DOI: 10.1017/CBO9781107337701.

[12] *Technical Information Manual MOD. N968 Spectroscopy Amplifier*. URL: https://www.caen.it/products/n968/.

[13] AN Zheng-Hua et al. *Experimental study on the performance of a single-THGEM gas detector*. 2010. DOI: 10.1088/1674-1137/34/1/015. URL: http://hepnp.ihep.ac.cn//article/id/b539b7ac-61f5-4e38-9627-6ed91572ee8f.

[14] P. A. Zyla et al. "Review of Particle Physics". In: *PTEP* 2020.8 (2020), p. 083C01. DOI: 10.1093/ptep/ptaa104.